Article

Cancer Cell

Critical Role for CD103$^+$/CD141$^+$ Dendritic Cells Bearing CCR7 for Tumor Antigen Trafficking and Priming of T Cell Immunity in Melanoma

Graphical Abstract

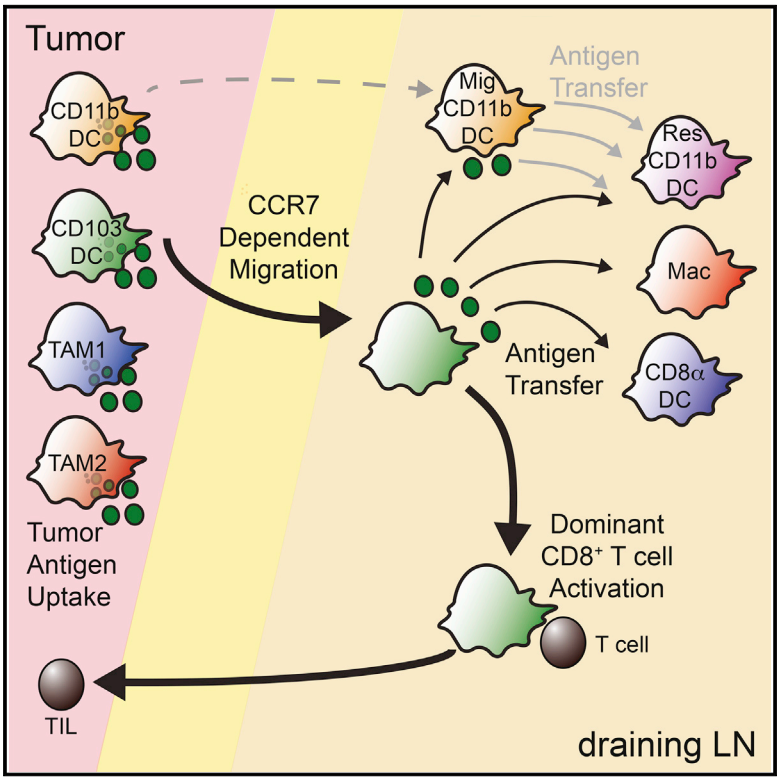

Authors

Edward W. Roberts, Miranda L. Broz, Mikhail Binnewies, ..., Dusan Bogunovic, Nina Bhardwaj, Matthew F. Krummel

Correspondence

matthew.krummel@ucsf.edu

In Brief

Roberts et al. show that intratumoral CD103$^+$ dendritic cells (DC) in mice, or CD141$^+$ DC in humans, traffic tumor antigens to lymph nodes to prime CD8$^+$ T cells, which requires CCR7 on these DC. High CCR7 expression level in human tumors correlates with signatures of CD141$^+$ DC and better clinical outcomes.

Highlights

- Tumor antigen trafficking and "painting" identify LN trafficking immune cells
- CD103$^+$ DC are critical tumor-draining antigen-presenting cells driving CD8$^+$ T cells
- CCR7 on CD103$^+$ DC is required for tumor antigen drainage and T cell activation
- CCR7 level in human melanoma correlates with T cell infiltration and patient survival

Roberts et al., 2016, Cancer Cell *30*, 1–13
August 8, 2016
http://dx.doi.org/10.1016/j.ccell.2016.06.003

CellPress

Please cite this article in press as: Roberts et al., Critical Role for CD103+/CD141+ Dendritic Cells Bearing CCR7 for Tumor Antigen Trafficking and Priming of T Cell Immunity in Melanoma, Cancer Cell (2016), http://dx.doi.org/10.1016/j.ccell.2016.06.003

Cancer Cell
Article

Critical Role for CD103+/CD141+ Dendritic Cells Bearing CCR7 for Tumor Antigen Trafficking and Priming of T Cell Immunity in Melanoma

Edward W. Roberts,[1,6] Miranda L. Broz,[1,6,7] Mikhail Binnewies,[1] Mark B. Headley,[1] Amanda E. Nelson,[1] Denise M. Wolf,[2] Tsuneyasu Kaisho,[3] Dusan Bogunovic,[4] Nina Bhardwaj,[5] and Matthew F. Krummel[1,*]
[1]Department of Pathology, University of California San Francisco, 513 Parnassus Avenue, San Francisco, CA 94143-0511, USA
[2]Department of Laboratory Medicine, University of California San Francisco, San Francisco, CA 94143, USA
[3]Institute of Advanced Medicine, Wakayama Medical University, Wakayama 641-8509, Japan
[4]Department of Microbiology
[5]Tisch Cancer Institute
Icahn School of Medicine at Mount Sinai, New York, NY 10029, USA
[6]Co-first author
[7]Present address: Precision Immune Inc, 953 Indiana Street, San Francisco, CA 94107, USA
*Correspondence: matthew.krummel@ucsf.edu
http://dx.doi.org/10.1016/j.ccell.2016.06.003

SUMMARY

Intratumoral dendritic cells (DC) bearing CD103 in mice or CD141 in humans drive intratumoral CD8+ T cell activation. Using multiple strategies, we identified a critical role for these DC in trafficking tumor antigen to lymph nodes (LN), resulting in both direct CD8+ T cell stimulation and antigen hand-off to resident myeloid cells. These effects all required CCR7. Live imaging demonstrated direct presentation to T cells in LN, and CCR7 loss specifically in these cells resulted in defective LN T cell priming and increased tumor outgrowth. CCR7 expression levels in human tumors correlate with signatures of CD141+ DC, intratumoral T cells, and better clinical outcomes. This work identifies an ongoing pathway to T cell priming, which should be harnessed for tumor therapies.

INTRODUCTION

CD8+ T cells, specifically cytotoxic T cell lymphocytes (CTLs), are a critical component of the protective immune response against tumors. Tumor-specific, antigen-experienced T cells can be found in most tumor tissue as well as circulating in mouse and human tumor patients (Robbins et al., 2013). The frequency and location of T cell infiltrates in tumors has strong prognostic value for survival in human patients (Galon et al., 2006). In many mouse models, anti-tumor immunity requires the generation of tumor-specific CTLs (Dunn et al., 2004) and it is similarly believed that CTLs, generated through lymph priming, are major players in successful immunotherapies of human cancers.

Draining lymph nodes (dLN) serve to organize immune responses by bringing antigen-presenting cells (APCs) and T cells together spatially and temporally to promote T cell proliferation. T cell priming in cancer similarly is thought to require a pool of specific tumor antigens that can be recognized by the host as well as an APC population capable of robust tumor antigen cross-presentation (Huang et al., 1994) that can move these antigens to the dLN. Although specific proteins mutated in tumor cells have been identified as antigenic targets of tumor-infiltrating T cells (Kawakami et al., 1994a, 1994b; Robbins et al., 2013), the identity of the APC(s) that move antigens to dLN and prime cells there remains unresolved.

Myeloid APCs, which include multiple subsets of dendritic cells (DC) and macrophages, are specialized cells that acquire,

Significance

Emerging cancer immunotherapies enhance the ability of T cells to reject tumors. While it is increasingly clear that myeloid antigen-presenting cells play both positive and negative roles in influencing intratumoral T cell expansion and function, the identity of populations and mechanisms of tumor antigen transfer responsible for LN priming of T cells remains obscure. Here, we have undertaken multiple labeling strategies to demonstrate that the majority of trafficking occurs via CCR7-dependent migration of the CD103+/CD141+ subset of DC. By identifying this population as a strong driver of T cell expansion and overall outcome in both mouse and human tumors, this work isolates this pathway as a strong partner for current and future immunotherapies.

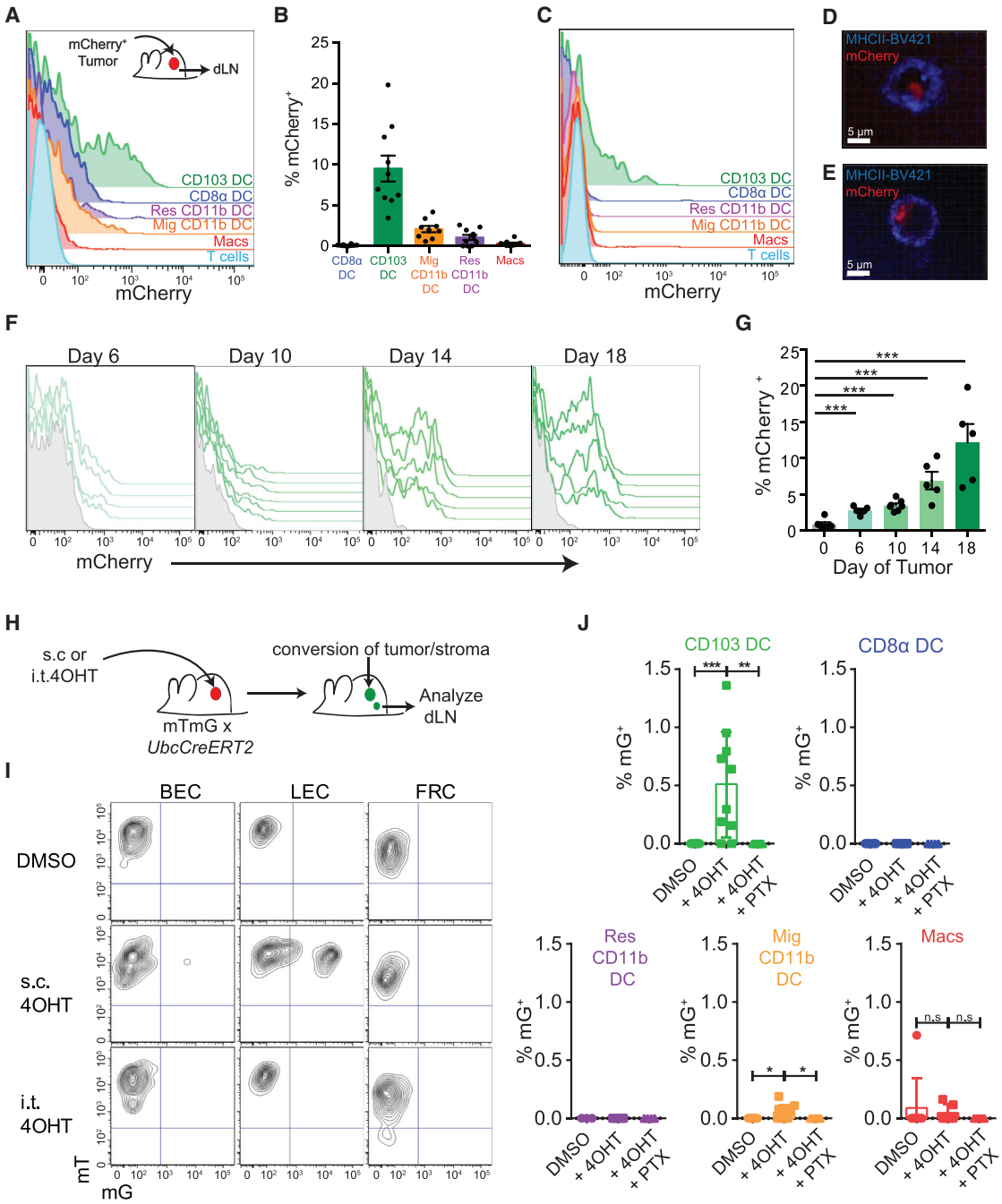

Figure 1. Migratory CD103+ DC Carrying Tumor Antigen Accumulate in the Tumor dLN

(A) Representative histogram of tumor-derived mCherry fluorescence across the tumor dLN populations of the inguinal and axillary LN in the ectopic B78ChOVA tumor model.

(B) Frequency of mCherry+ DC populations across the tumor dLN of multiple B78ChOVA tumors. Data were pooled from dual-flank-bearing tumor animals and plotted as mean ± SEM for each population (n = 5). Mig, migratory; Res, resident, Macs, macrophages.

(C) Representative histogram of tumor-derived mCherry florescence across the tumor dLN populations of the inguinal and axillary LN in the spontaneous PyMTChOVA breast tumor model.

(D and E) Representative confocal image of sorted CD103+ DC from tumor dLN (D) or primary tumor (E) of B78ChOVA-bearing mice. Cell membranes labeled with brilliant violet 421-conjugated MHC class II antibody are shown in blue with tumor-derived mCherry fluorescence in red.

(F) Representative flow cytometric histograms of tumor-derived mCherry fluorescence within the CD103+ DC populations in the tumor dLN of tumor-bearing animals over tumor progression from day 6 through day 18. Data are from dual-flank-bearing tumor animals from the left and right inguinal and axillary dLN (n = 3). Overlays represent individual LN.

(legend continued on next page)

process, and present antigens to naive T cells for the induction of antigen-specific immune responses. Within the LN, DC can be grouped as either LN resident, which include CD8α^+ and CD11b$^+$ resident DC, or migratory, which include CD103$^+$ and CD11b$^+$ migratory DC. The LN is also populated with specialized populations of macrophages, including CD169$^+$ subcapsular macrophages and occasionally with monocyte-derived macrophages, sometimes called moDC or inflammatory DC (iDC) that share similar features with DC. Previously, using *Batf3*$^{-/-}$ mice deficient for both CD103$^+$ and CD8α^+ DC, it was observed that one or both of these are required for cytotoxic T cell immunity and ultimately for rejection of highly immunogenic tumors (Hildner et al., 2008). Another report demonstrated that CD169$^+$ macrophages played a key role in the priming of T cells in response to injected apoptotic tumor cells (Asano et al., 2011). However, the complete pathway of antigen transfer from tumor to dLN APCs for presentation to T cells in the context of a growing tumor has not been carefully dissected.

Previously, we identified a critical role for intratumoral CD103$^+$ DC in T cell repriming and adoptive T cell therapy, specifically at the tumor site (Broz et al., 2014). These DC have homologous populations in human tumors, which are defined by expression of CD141 (also known as BDCA3 [Haniffa et al., 2012]). Here, we aimed to extend these findings to explore the mechanisms of antigen transfer to the dLN necessary for the generation of tumoral T cell infiltrate.

RESULTS

Progression and Dissection of the Tumor-Draining LN Environment

To dissect the APC compartment of the tumor dLN, we utilized a 12-color flow cytometry panel to identify the unique DC and macrophage subsets from both healthy and tumor dLN. We identified populations including resident CD8α^+ DC, resident CD11b$^+$ DC, migratory CD11b$^+$ DC, CD103$^+$ DC, and rare macrophages (Figures S1A and S1B). We applied this approach to mice bearing the B78ChOVA melanoma (Broz et al., 2014), a variant of B16-F10 (Fidler, 1975) engineered to express both ovalbumin as a neo-tumor antigen as well as the fluorescent mCherry protein to track antigen uptake by phagocytes. Using this tumor, which grows progressively in immunocompetent mice, we tracked the changes within the LN during tumor development and found a steady decrease in all APC subsets as a fraction of all LN cells, despite a general increase in overall dLN cellularity (Figures S1C–S1F). This reduction in frequency was not due to the arrival of metastatic tumor cells in the LN, as CD45$^-$ mCherry$^+$ cells were not found in dLN even at late time points. We also observed this trend in multiple other tumor models including those that arise spontaneously due to tissue-specific oncogene expression (e.g., Engelhardt et al., 2012). It was against this backdrop that we sought to track the mechanisms that carried antigens to the dLN in progressively growing tumors.

Migratory CD103$^+$ DC Is the Dominant Cell Type that Carries Antigen to the dLN

To track the population(s) of APC in the dLN that had originated in the tumor microenvironment, we undertook two complementary approaches. First, we implanted B78ChOVA tumors subcutaneously and, by flow cytometry, identified all dLN cells that displayed mCherry fluorescence. At day 15 after implantation a significant proportion of CD103$^+$ DC, typically 10%–15%, were mCherry$^+$ in tumor dLN (Figures 1A and 1B). In contrast, only modest proportions of other myeloid populations were mCherry$^+$ with ~3% of CD11b$^+$ migratory DC, ~1% of resident CD11b$^+$ DC, and <0.5% of LN macrophages displaying mCherry fluorescence. We found the same profound bias in another ectopic mouse model of cancer (Figure S1G) and also in a spontaneous breast tumor model, PyMTChOVA (Engelhardt et al., 2012) (Figure 1C), which suggests that this was not an artifact of the injection route or abnormal features of this particular tumor microenvironment.

mCherry$^+$ CD103$^+$ DC were also sorted from the dLN and tumors of tumor-bearing mice and imaged using confocal microscopy. Vesicularized intracellular mCherry fluorescence could be identified in cells from both the dLN (Figure 1D) and the primary tumor (Figure 1E), confirming that CD103$^+$ DC had engulfed tumor antigen. While other studies, using apoptotic tumor cell injections, have suggested CD169$^+$ macrophages as important tumor dLN APCs, we did not observe them to be loaded in progressively growing tumors; however, we did confirm their loading when tumors were irradiated prior to injection and LN were isolated a day after the injection (Figures S1H–S1J). Such loading may therefore result from bolus drainage of dead cells from the injection site. The tumor antigen loading of CD103$^+$ DC also increased as tumors grew (Figure 1F), rising from 2% to 5% of CD103$^+$ DC in the dLN at early time points to 12%–15% at late tumor stages (Figure 1G).

Since it was possible that this method failed to capture cells that completely digested the tumor-intrinsic fluorophore, we devised a second lineage-tracing method for tracking the migration of APCs from tumor to LN. We crossed mTmG mice in which cells expressing active Cre change from tdTomato$^+$ (mT) to GFP$^+$ (mG) (Muzumdar et al., 2007) to *Ubc-CreERT2* mice in which Cre moves to the nucleus and becomes active in the presence of 4-hydroxy-tamoxifen (4OHT) (Indra et al., 1999). We then introduced tumors into these mice and administered 4OHT by injection either intratumorally or subcutaneously (Figure 1H). Controls received vehicle alone (DMSO) intratumorally. We then analyzed

(G) Frequency of mCherry$^+$ CD103$^+$ DC in the tumor dLN over tumor progression. Data were pooled from dual-flank-bearing tumor animals, and plotted as mean ± SEM for each population at each time point compared with a healthy animal on day 0 (n = 3). ***p < 0.001.

(H) Schematic showing the method of labeling tumor stroma by intratumoral injection of 4OHT in *UbcCreERT2* mTmG mice bearing B16F10 tumors.

(I) Representative flow cytometric plots showing mG fluorescence of LN stromal populations when 4OHT or vehicle is administered intratumorally or subcutaneously. Data are representative of five independent experiments.

(J) Histograms showing marking of tumor dLN myeloid populations 24 hr after three daily intratumoral injections of 4OHT treated with 0.5 μg of either PTX or PBS 4 hr prior to each injection with 4OHT (n ≥ 4 for all groups).

Plots show mean ± SEM. Data are representative of five independent experiments. *p < 0.05, **p < 0.01, ***p < 0.001. n.s, not significant. See also Figure S1.

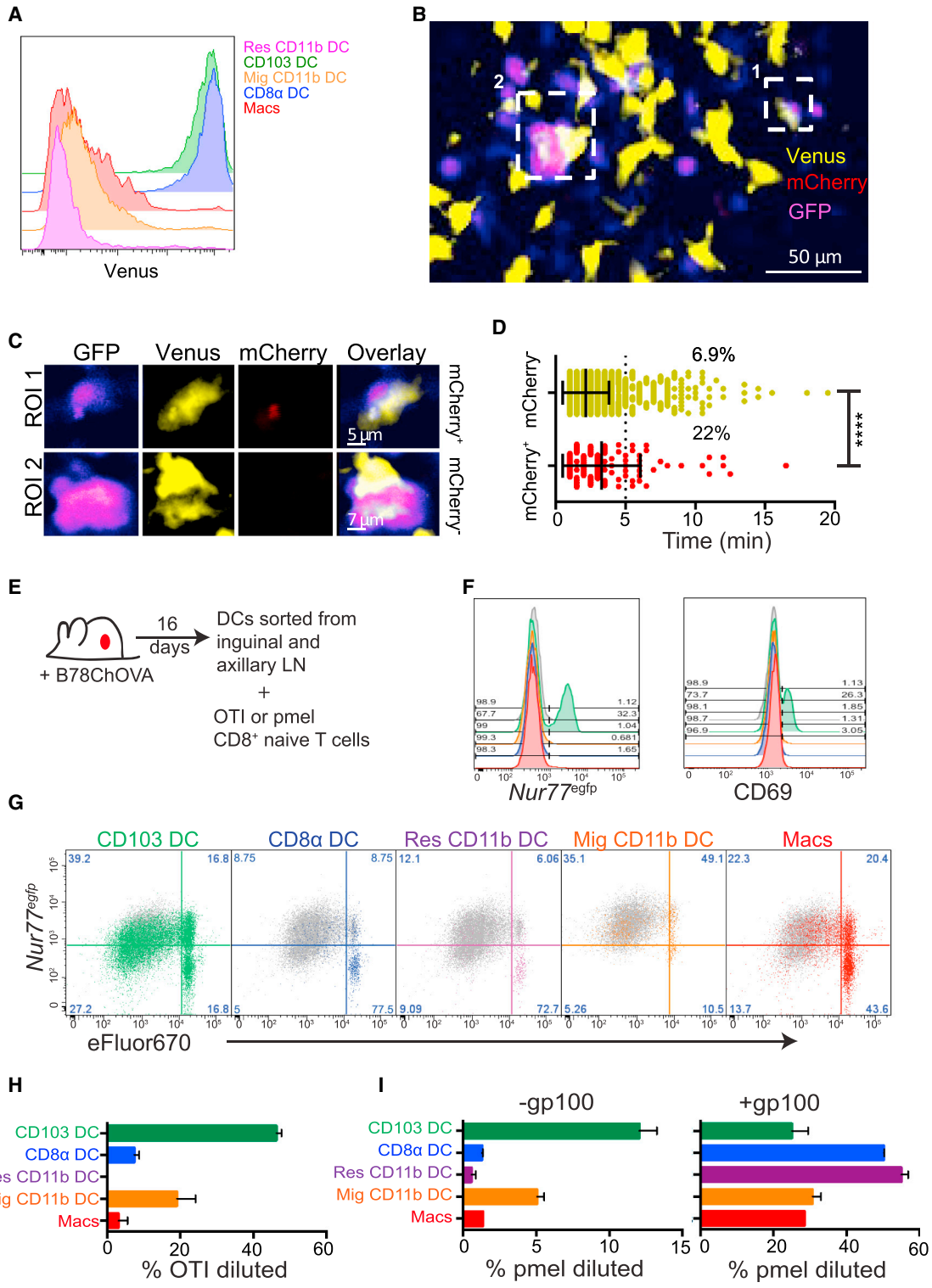

Figure 2. Several Tumor dLN Myeloid Populations Stimulate Naive OTI Proliferation In Vitro

(A) Representative flow cytometric plot showing expression of the Venus transgene within the myeloid populations in the tumor dLN.

(B) Time projection of representative multiphoton microscopy image of tumor dLN explants of B78ChOVA-bearing *Xcr1*-Venus mice 2 days after transfer of 2×10^6 GFP$^+$ OTI T cells. XCR1$^+$ cell time projections are represented in yellow, OTI T cells in blue, and mCherry in red. Two regions of interest (ROI) are shown.

(C) Time projection of the XCR1$^+$ DC and interacting OTI T cells in ROI 1 and ROI 2.

(legend continued on next page)

the LN stroma to ensure that our intratumoral injections were not delivering the 4OHT directly to the LN. Although subcutaneous injections resulted in robust conversion from mT^+ to mG^+ in a portion of the lymphatic endothelium and occasionally small fractions of the blood endothelium, we never observed this direct drainage with intratumoral injections (Figure 1I). We verified that the 4OHT was not directly draining to the dLN for all subsequent experiments, permitting us to then ask which immune populations, labeled specifically in tumors, migrate to the LN.

When we analyzed mG^+ cells in the dLN after three doses of 4OHT given daily, we found that while 0.5%–1% of total $CD103^+$ DC were routinely labeled, there was no detectable labeling of $CD8\alpha^+$ DC or resident $CD11b^+$ DC and less than 0.1% labeling of migratory $CD11b^+$ DC (Figure 1J). The proportion of $CD103^+$ DC labeled was comparable with that labeled in the tumor, where approximately 1% of cells were labeled in various populations (Figure S1K). While LN macrophages were occasionally autofluorescent, there was no statistically significant increase in macrophage labeling with 4OHT. For both $CD103^+$ DC and the minimal $CD11b^+$ DC migration, injection of pertussis toxin (PTX) into mice during the assay, which blocks $G\alpha_i$ signaling and thus many types of chemokine-dependent migration, completely abrogated labeling in the LN (Figure 1J).

While both of these assays lack the ability to measure subtle trafficking of either antigen or cells, both support the existence of prominent $CD103^+$ DC movement, from tumor to the dLN, with much less traffic of other cell types, prompting us to question which cell types were critical for mediating LN priming.

$CD103^+$ DC Interact with Tumor-Specific T Cells in the dLN

The amplification of tumor-specific T cells (tumor-infiltrating lymphocytes [TILs]) in both mice and humans is a very well studied phenomenon in cancer, despite their apparent ineffectuality in tumor eradication. However, the source of initial T cell LN priming is still unclear. Based on the trafficking data in Figure 1, and observations of poor tumor control in *Batf3*$^{-/-}$ animals lacking $CD103^+$ and $CD8\alpha^+$ DC (Fuertes et al., 2011; Hildner et al., 2008), we hypothesized that the $CD103^+$ DC were, in fact, the population of APC responsible for anti-tumor T cell priming. Since $CD103^+$ and $CD8\alpha^+$ DC both express the chemokine receptor XCR1 and of these cells only $CD103^+$ DC are $mCherry^+$, we used an *Xcr1*-Venus allele together with mCherry positivity to determine whether antigen-bearing $CD103^+$ DC form synapses with naive T cells in the tumor dLN in vivo. We first confirmed that both $CD8\alpha^+$ DC and $CD103^+$ DC are XCR1 positive and that this correlates with Venus expression in the LN (Figure 2A). We then introduced B78ChOVA tumors into *Xcr1*-Venus mice, and adoptively transferred GFP-expressing naive OVA-reactive OTI $CD8^+$ T cells. 48 hr later we imaged live tumor dLN explants by two-photon microscopy to determine whether $XCR1^+$ cells were mediating T cell arrest. In Figure 2B, we highlight two regions of interest (ROI) containing direct T cell-DC contacts within a larger field comprising the T cell zone. This time projection across the full 30 min of real-time acquisition shows a pseudocolor scale where purple represents areas where T cells are present for long periods of time (Figure 2B). Both of these regions can be seen to be "hotspots" for T cell arrest and are both nucleated by a $Venus^+$ cell. GFP^+ OTI T cells were found to interact with $mCherry^+$ $Venus^+$ cells ($CD103^+$ DC) as well as $mCherry^-$ $Venus^+$ cells (Figure 2C and Movie S1). However, the average interaction time for T cells with the $mCherry^+$ $XCR1^+$ ($CD103^+$ DC) cells were significantly longer than those with $mCherry^-$ $Venus^+$ cells, and 22% of T-DC interactions exceeded 5 min for the $mCherry^+$ DC compared with 6.9% for the $mCherry^-$ DC (Figure 2D), indicating that the $CD103^+$ DC carrying tumor antigen were capable of inducing stable motility arrest of OTI T cells in the dLN. We note that mCherry levels may be below the detection limit of two-photon microscopy, since the proportion of $mCherry^+$ $XCR1^+$ DC was much lower in these experiments than was found by the more sensitive flow cytometric measurements (Figures 1A and 1B); failure to detect these cells may bias our measurements of the extent of their T cell engagement.

Robust LN Priming by $CD103^+$ DC and Evidence for Antigen Hand-Off to Resident APC Populations

To directly test which LN populations were capable of robustly stimulating tumor-specific T cells, we isolated $CD8\alpha^+$ DC, $CD11b^+$ DC migratory and resident, $CD103^+$ DC, and macrophages from the dLN of B78ChOVA tumor-bearing mice and assayed their ability to activate naive OTI T cells in vitro, without the addition of exogenous antigen (Figure 2E). At 12 hr, only the $CD103^+$ DC from the dLN induced the early activation of T cells, as measured by CD69 and *Nur77*^{EGFP} induction (Figure 2F). When assessed for cell division by dye dilution at 72 hr, the $CD103^+$ DC were again the most robust stimulators of OTI T cell proliferation, both in percent diluted as well as total T cells recovered. Migratory $CD11b^+$ DC also drove a lower, but still substantial degree of OTI proliferation, however, these resulted in much lower total T cell recovery, particularly in the divided fraction (Figures 2G and 2H). This latter distinction may be a result of decreased survival or enhanced apoptosis

(D) Representative OTI T cell dwell time on $XCR1^+$ population determined by mCherry fluorescence within the dLN. Data are plotted as median ± interquartile range and statistics were performed using the Mann-Whitney U test. ****$p < 0.0001$.

(E) Schematic of T cell activation assay with sorted populations from the dLN of B78ChOVA tumor-bearing mice.

(F) Representative flow cytometric histograms of the induction of *Nur77*^{EGFP} transgene and the early activation marker CD69 by OTI T cells cultured for 12 hr on APCs sorted directly from the tumor dLN of mice. $CD103^+$ DC is green, migratory $CD11b^+$ DC orange, resident $CD11b^+$ DC purple, $CD8\alpha^+$ DC blue, and macrophage red. Data are representative of three independent experiments.

(G) Representative flow cytometric plots of naive OTI T cell proliferation, as measured by dye dilution of eFluor 670 plotted against *Nur77*^{EGFP}, at 72 hr following co-culture with tumor dLN APC populations. Gray, BM-derived DC + OTI cognate peptide (SL8). Data are representative of four independent experiments.

(H) Proportion of OTI T cells at 72 hr that have divided following co-culture with tumor dLN APC populations. Plots show mean ± SEM. Data are representative of four independent experiments.

(I) Proportion of pmel T cells at 72 hr that have divided following co-culture with tumor dLN APC populations ± addition of gp100 peptide. Plots show mean ± SEM. Data are representative of two independent experiments.

See also Movie S1.

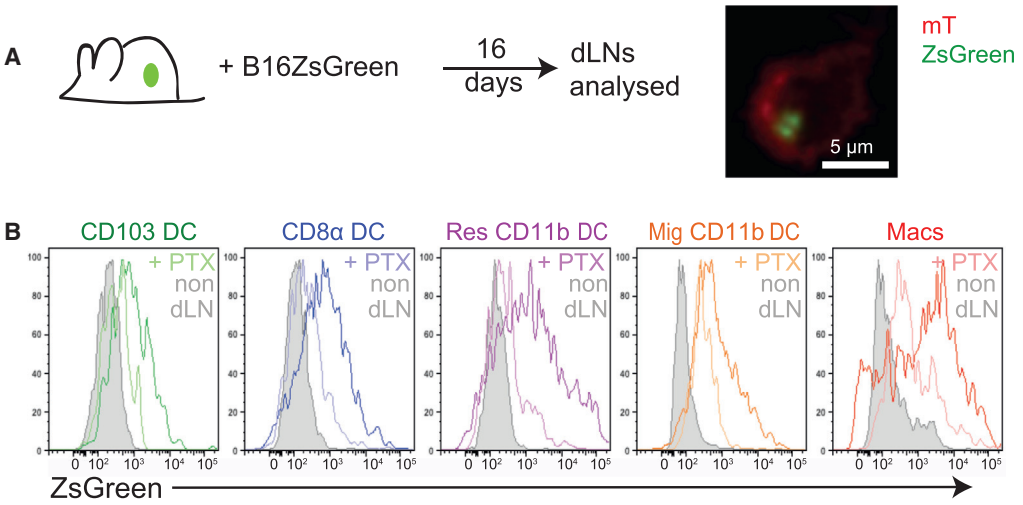

(legend on next page)

concomitant with the weaker proximal signaling indicated by CD69 and *Nur77*^{EGFP}. To confirm that this was not an artifact of the high affinity of the OTI system for its cognate antigen, we repeated this analysis using pmel T cells that recognize the gp100 peptide in B16 melanoma cells. The same pattern was seen with the pmel system whereby CD103$^+$ DC were the most robust stimulators of CD8$^+$ T cells (Figure 2I). Furthermore, upon addition of gp100 peptide all myeloid subsets were seen to be robust stimulators of pmel CD8$^+$ T cells, suggesting that all subsets had the capacity to stimulate naive CD8$^+$ T cells, but only the CD103$^+$ and migratory CD11b$^+$ DCs were in fact endogenously presenting tumor antigen in the dLN, the former more significantly than the latter (Figure 2I).

While in vitro assays do not fully represent the situation occurring in vivo, they clearly indicate increased T cell stimulation capacity for the CD103$^+$ DC and to a lesser extent the migratory CD11b$^+$ DC. However, given our trafficking data, we were surprised by the consistent observation of modest stimulation of T cells by CD8α^+, CD11b$^+$ resident DC, and macrophage populations as evidenced by small numbers of cells in the dye-diluted pools as well as the induction of *Nur77*^{EGFP} at later time points (Figure 2G). Based on the cellular trafficking of Figure 1, this would not be expected unless antigens were passed between the trafficking populations and the resident populations as has previously been observed in skin-infection models (Allan et al., 2006), or if antigens were passively draining to the dLN in lymphatics.

CD103$^+$ DC Tumor Antigen Trafficking to the LN Is CCR7 Dependent

To provide a greater possibility to track antigens that might be degraded during hand-off or transit, we engineered another variant melanoma line, this time taking the parental B16 melanoma cell line and introducing the bright and highly stable fluorophore ZsGreen (Nakamura et al., 2013), which is documented to resist both low pH and lysosomal degradation (Katayama et al., 2008), and which we have confirmed to be significantly less subject to degradation when ingested by phagocytes (data not shown). When we introduced these tumors into mice and removed dLN to analyze the myeloid populations, similarly to the previous assays we found that the fluorophore was again compartmentalized within CD103$^+$ DC (Figure 3A). However, we now also found that we could detect fluorescence by flow cytometry in all the remaining myeloid populations in the LN, with quantitatively greatest levels in the macrophages and resident CD11b$^+$ DC (Figure 3B). Since these did not themselves traffic to this extent (Figure 1), we hypothesized that antigen-containing compartments might be shared with other APCs by some form of transport (Allan et al., 2006) or that stable ZsGreen drained directly into the LN. Using the fluorescent-antigen tracking method, we observed that the accumulation of mCherry$^+$ CD103$^+$ DC in dLN was PTX sensitive (Figure S2A). Likewise, in the context of the more stable ZsGreen fluorophore, accumulation of fluorescence by all cell types was PTX sensitive (Figure 3B). Both were consistent with the hypothesis, above, that this more stable antigen is being brought into the LN in a chemokine signaling-dependent manner and is not simply passively draining in lymphatics.

Conventional DC LN trafficking is driven by the chemokine receptor CCR7 (Ohl et al., 2004). Therefore, we assayed the expression of *Ccr7* within intratumoral APCs (Figure S2B) and found that CD103$^+$ DC have ~5 -fold higher levels of *Ccr7* transcript than CD11b$^+$ DC and approximately 100-fold higher levels than tumor-associated macrophage (TAM) populations. Analysis of cell surface CCR7 level showed selective expression in intratumoral CD103$^+$ DC. Approximately one-third of CD103$^+$ DC expressed CCR7, perhaps representing variations in maturation state (Figure 3C). Comparatively, 100% of CD103$^+$ and CD11b$^+$ migratory DC in tumor dLN expressed high levels of CCR7 protein on their surface (Figure S2C).

When B78ChOVA tumors were introduced into *Ccr7*$^{-/-}$ animals, CD103$^+$ DC and CD11b$^+$ migratory DC were approximately 10-fold reduced in total dLN compared with controls (Figures 3D and 3E). We also found that while *Ccr7* deficiency did not lead to deficits in DC frequencies within tumors (Figure S2D) nor in their ability to take up tumor antigen and become mCherry positive (Figure S2E), it did lead to nearly complete loss of ZsGreen$^+$ cells within dLN populations when the tumor expressed the more stable ZsGreen fluorophore (Figure 3F) and, similarly, loss of detectable mCherry fluorescence when tumors expressed this protein (Figure S2F).

CCR7 Dependence of T Cell Priming in the Tumor dLN

Given these observations, we sought to address the consequence of CCR7 loss for the ability of a tumor dLN to support naive CD8$^+$ T cell priming and proliferation. Since CCR7 is also required for T cells to enter the LN, we devised a system in which *Ccr7*-sufficient OTI T cells were adopted into wild-type (WT) or *Ccr7*$^{-/-}$ mice (Figure 4A). Doing this, we observed that T cells in *Ccr7*$^{-/-}$ mice displayed a significantly diminished activation

Figure 3. Tumor Antigen Arrival in All Tumor dLN DC Populations Is CCR7 Dependent

(A) Schematic of assessment for LN drainage of the pH-stable fluorophore ZsGreen and representative confocal image of sorted CD103$^+$ DC from tumor dLN of B16 ZsGreen-bearing mTmG mice. Cell membrane is labeled with membrane bound tdTomato in red and tumor-derived ZsGreen fluorescence in green.

(B) Representative histogram of tumor-derived ZsGreen florescence across the tumor dLN populations of the inguinal and axillary LN in the ectopic B16 ZsGreen melanoma tumor model treated with 0.5 μg of either PTX (paler line) or PBS (darker line) for 5 days compared with the non-dLN (gray). Data are representative of two independent experiments.

(C) Representative flow cytometric histograms of CCR7 levels on tumor myeloid populations and T cells (colored) compared with isotype control (gray) (n = 3).

(D) Representative flow cytometric plot of CD8α^+ and CD103$^+$ DC in the tumor dLN of either WT or *Ccr7*$^{-/-}$ mice. Cells shown were gated as CD11c$^+$, MHC class II$^+$, F4/80$^-$, Ly6C$^-$, CD90.2$^-$, and B220$^-$.

(E) Frequency of DC populations as a percentage of total live cells in the tumor dLN of WT or *Ccr7*$^{-/-}$ mice. Pooled data from individual mice with dual-flank tumors are presented as mean ± SEM for each population (n = 3), and are representative of three independent experiments. *p < 0.05, **p < 0.01, ***p < 0.001.

(F) Quantification of the proportion of total myeloid populations that are ZsGreen$^+$ within the tumor dLN in the presence or absence of CCR7. Data are presented as mean ± SEM for each population (n = 5) and are representative of two independent experiments. *p < 0.05, **p < 0.01.

See also Figure S2.

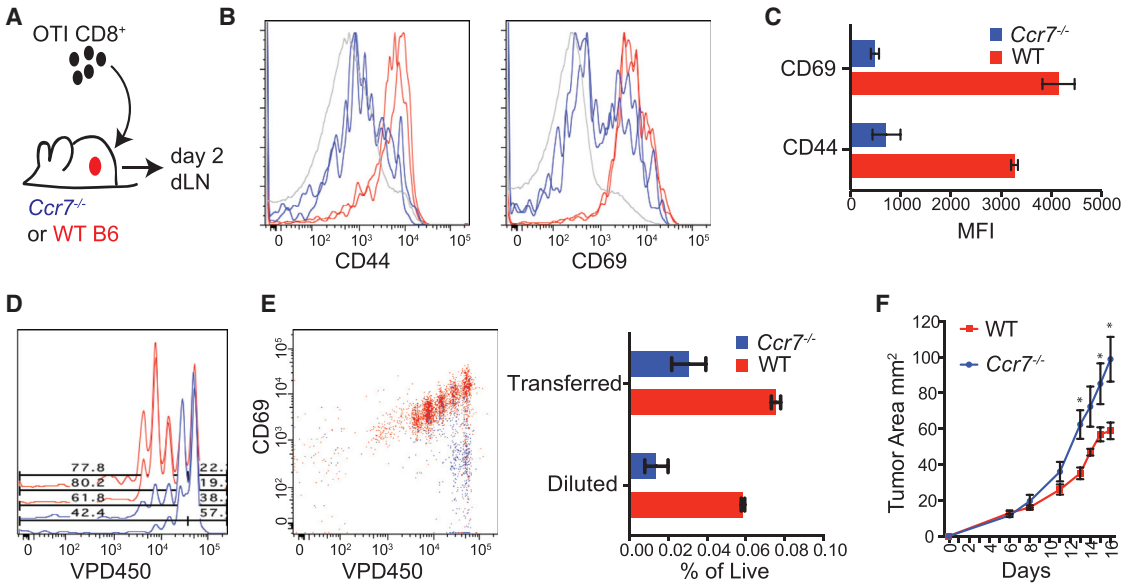

Figure 4. CCR7-Dependent Trafficking of Tumor Antigen to the Tumor dLN Is Required for Anti-Tumor T Cell Priming In Vivo

(A) Schematic of adoptive transfers of labeled T cells into tumor-bearing WT or *Ccr7*$^{-/-}$ mice for dLN analysis.

(B) Representative flow cytometric histogram of CD44 and CD69 expression on transferred T cells in the tumor dLN after 48 hr from either WT (red) or *Ccr7*$^{-/-}$ (blue) mice, with endogenous T cells in gray. Duplicate histogram overlays represent individual mice. Data are representative of two independent experiments.

(C) Quantified geometric mean fluorescent intensity of CD69 and CD44 expression of transferred OTI T cells in the tumor dLN of WT or *Ccr7*$^{-/-}$ mice at 48 hr. Data are presented as mean ± SEM (n = 3) and are representative of two independent experiments.

(D) Representative flow cytometric plots of proliferation measured by dye dilution of adoptively transferred OTI T cells in the dLN of tumor-bearing WT (red) or *Ccr7*$^{-/-}$ (blue) mice 2 days following transfer.

(E) Representative flow cytometric plots of dye dilutions of adoptively transferred OTI T cells in the dLN of tumor-bearing WT (red) or *Ccr7*$^{-/-}$ (blue) mice following transfer and plotted against CD69 expression. Quantified frequencies, as a percentage of total live LN cells, are plotted for the proportion of recovered transferred T cells (Transferred) as well as the proportion of those transferred T cells that divided (Diluted). Data were pooled from dual-flank-bearing tumor animals, and plotted as mean ± SEM (n = 3). Data are representative of two independent experiments.

(F) Tumor growth curves for ectopic B78ChOVA tumors in *Ccr7*$^{-/-}$ or aged-matched WT C57BL/6 mice over 16 days (without adoptively transferred T cells). Data are presented as tumor area and plotted as mean ± SEM (n = 5). *p < 0.05.

profile as measured by expression of CD69 and CD44 (Figures 4B and 4C). In addition, transferred T cells failed to proliferate in the dLN as indicated by dilution of a vital dye, VPD450, measured after 2 days (Figure 4D). When VPD450 versus CD69 upregulation was used to measure the percentage of divided cells, we found that there was a nearly 5-fold reduction in the number of diluted cells recovered from dLN in *Ccr7*$^{-/-}$ mice compared with WT controls (Figure 4E).

Despite the rapid growth of these tumors in WT hosts, loss of CCR7 led to even faster tumor growth (Figure 4F). Taken together, these results suggest that ongoing priming of new T cell clones and concomitant immune pressure on tumor growth is dependent upon the continual trafficking of antigens by specific DC populations through a CCR7-dependent pathway to the LN. However, as CCR7 deficiency also leads to defects in LN architecture and loss of other cellular subsets from the dLN, we sought to more specifically assess the role of CCR7 within the CD103^{+} DC compartment. To this end we created mixed bone marrow (BM) chimeras consisting of 50% *Xcr1*-DTR BM, where cells expressing *Xcr1* express the primate diphtheria toxin receptor (DTR) allowing their selective ablation, and 50% *Ccr7*$^{-/-}$ or WT BM. In these mice, 50% of all immune cells derive from *Ccr7*$^{-/-}$ BM while the other 50% are *Ccr7*$^{+/+}$ but contain the *Xcr1*-DTR transgene; this means that in the absence of diphtheria toxin (DT) treatment, 50% of all immune cells may traffic to the LN normally, but upon administration of DT all *Ccr7*$^{+/+}$ XCR1^{+} cells are ablated. Within the tumor, only the *Xcr1*-DTR BM-derived CD103^{+} DC are ablated, leaving the *Ccr7*$^{-/-}$ CD103^{+} DC compartment intact (Figure S3A). As such, the role of CD103^{+} DC within the dLN could be parsed from their previously demonstrated important roles in the tumor microenvironment. Similarly, within the lymph node, *Xcr1*-DTR BM-derived CD8α^{+} DC are ablated, leaving the *Ccr7*$^{-/-}$ CD8α^{+} DC intact (Figure S3B). The migratory CD11b^{+} DC from the *Ccr7*$^{-/-}$ BM fail to migrate to the dLN but those derived from the *Xcr1*-DTR BM do migrate and are not ablated, resulting in intact migration of these DC. Conversely, the CD103^{+} DC within the LN are completely lost since those derived from the *Ccr7*$^{-/-}$ BM fail to migrate to the dLN and those from the *Xcr1*-DTR BM are ablated (Figure S3C). In this way, administration of DT selectively removed the CD103^{+} DC compartment from the dLN.

Low numbers of OTI cells were transferred into these mice before being injected with B78ChOVA tumors. DT was administered throughout tumor development, and at day 15 the dLN and tumors were harvested to determine the number of OTI cells present in both compartments (Figure 5A). In the presence of DT, while the proportion of the dLN consisting of T cells was only marginally affected (Figure 5B), the generation of the anti-tumor

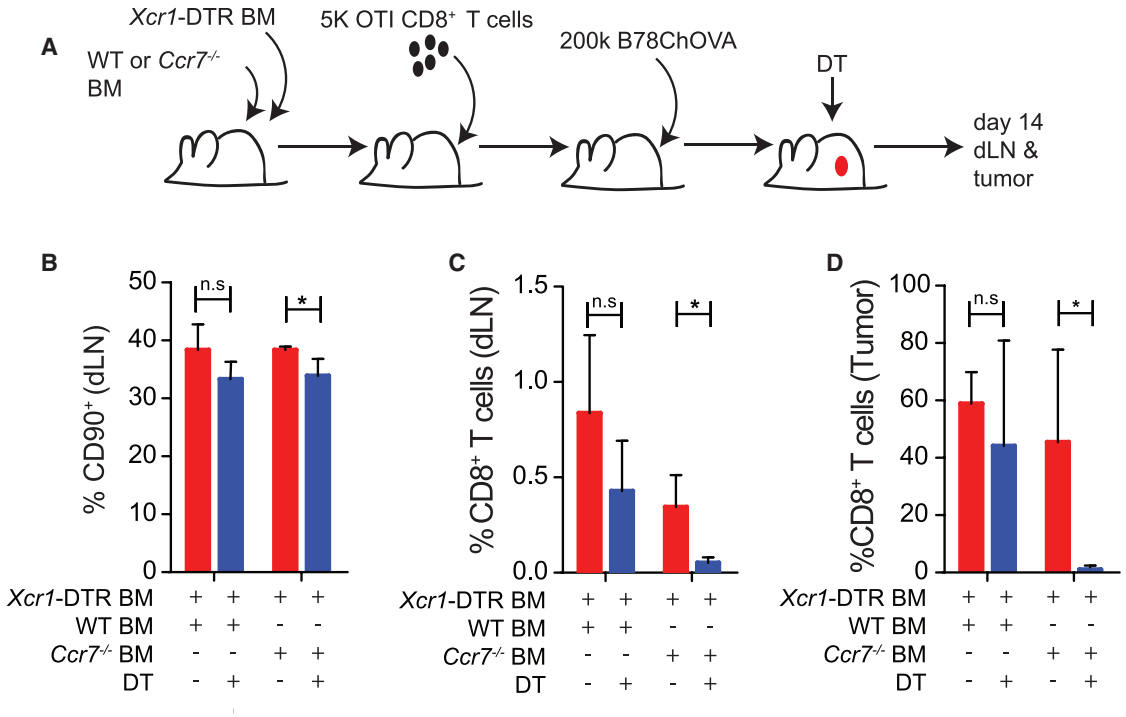

Figure 5. Migratory CD103+ DC Are Required in the dLN for Effective Anti-Tumor CD8+ T Cell Priming

(A) Schematic of adoptive transfers of 5,000 CD45.1+ OTI T cells into *XCR1-DTR*:*Ccr7*$^{-/-}$ mixed BM chimeras for analysis of TIL expansion ± elimination of CD103+ DC in the dLN.

(B) Proportion of live cells in the dLN that are CD90+ T cells 15 days after B78ChOVA inoculation in *XCR1-DTR*:WT and *XCR1-DTR*:*Ccr7*$^{-/-}$ mixed BM chimera ± DT treatment throughout tumor growth. Data are presented as mean ± SEM (n = 5).

(C and D) Proportion of CD8+ T cells in the dLN (C) or tumor (D) from the transferred CD45.1+ OTI T cells 15 days after B78ChOVA inoculation in *XCR1-DTR*:WT and *XCR1-DTR*:*Ccr7*$^{-/-}$ mixed BM chimera ± DT treatment throughout tumor growth. Data are presented as mean ± SEM (n = 5).

*p < 0.05; n.s, not significant. See also Figure S3.

OTI T cell response was dramatically impaired in the absence of CD103+ DC migration (Figure 5C). More critically, this corresponded to a loss of the OTI T cell response within the primary tumor, where the OTI T cell response was almost undetectable within the CD8+ T cell compartment (Figure 5D), indicating that migration of CD103+ DC to the LN and naive priming there is the critical determinant of generating effective anti-tumor CD8+ T cell responses in the LN and the tumor.

A CCR7-DC Axis Is Critical for Regulating T Cell Infiltration and Disease Progression in Human Melanoma

To put this work in the context of human melanoma, we queried databases containing expression profiles from individual human lesions. In previous work, we identified both *IRF8* and *FLT3* as "signature genes" for the human equivalents of the CD103+ DC population (Broz et al., 2014); in humans these are defined by expression of XCR1 as in mouse, but express CD141 (BDCA3) rather than CD103 (Haniffa et al., 2012). We previously also described *CCR7* as one of these signature genes (Broz et al., 2014), without understanding the full import of this association. Now, by assessing individual patient biopsy expression data, we observed a correlation between *IRF8* and *CCR7* and between *FLT3* and *CCR7* in both a 44-patient cohort dataset that contains significant pathology and outcome data (Bogunovic et al., 2009) (Figure 6A) and a recent TCGA dataset (Figures S4A and S4B). Such a correlation is consistent with the hypothesis that tumoral *Ccr7* expression is contained within the CD141+ DC subset. To directly test this, we isolated cells from fresh human melanoma biopsies and analyzed CCR7 levels on different tumor-infiltrating populations by flow cytometry. We found that only the CD141+ DC expressed detectable surface CCR7 (Figure 6B). This demonstrated that CCR7 is particularly prominent on CD141+ DC in human tumors and therefore is likely to represent the same axis of presentation that we observed in mouse. We noted that, as in mouse, the population was bimodal, perhaps suggesting that a maturation event takes place within this population, leading to upregulation of CCR7 and subsequent trafficking.

Finally, we sought to determine whether *CCR7* expression, and thus antigen-trafficking capacity, also predicted the generation of large numbers of TILs and had any correlation with patient survival. In the TCGA dataset, intratumoral *CCR7* expression was highly correlated with tumoral *CD3E* expression (Figure S4C). In the 44-patient cohort, we found that a median split for the *CCR7* expression also strongly correlated with CD3+ T cell infiltration, measured histologically (Figure 6C). More relevant to immune surveillance, the same median split provided a highly significant parsing of patient outcome; whereas the *CCR7*^{lo} cohort had perished by 1,250 days, 65% of the *CCR7*^{hi}

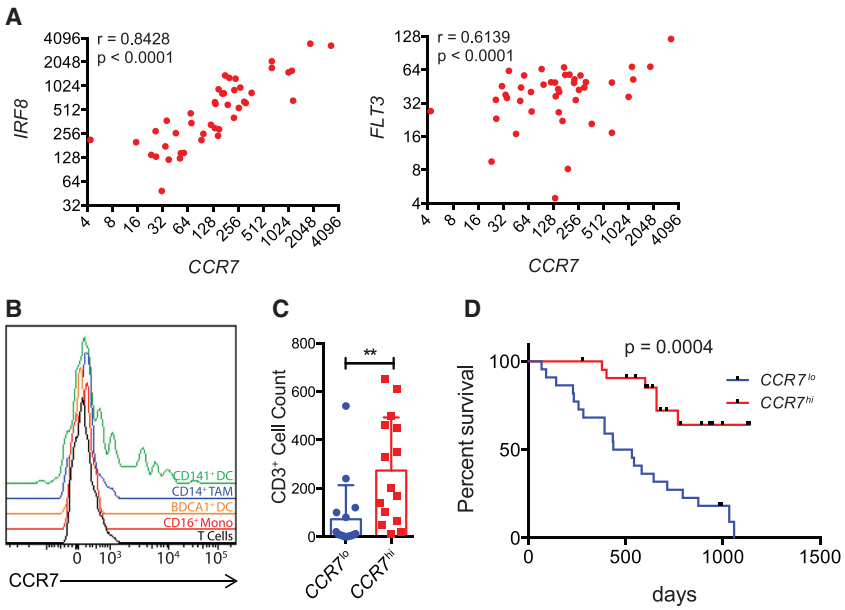

Figure 6. High Expression of *CCR7* Correlates with Greater T Cell Infiltration in Human Melanoma and Better Patient Outcomes

(A) Scatterplot showing *CCR7* transcript levels from 44 human melanoma samples against the transcript levels of *IRF8* and *FLT3*. Pearson correlation coefficient is shown.

(B) Representative flow cytometric plots of CCR7 levels on tumor immune populations from a fresh human metastatic melanoma biopsy.

(C) Histogram showing $CD3^+$ T cell counts from 44 human melanoma samples with less than median *CCR7* expression ($CCR7^{lo}$) or above median CCR7 expression ($CCR7^{hi}$). T cells were counted on histological slides by microscopy. Data are presented as mean ± SEM. **p < 0.01.

(D) Survival curve of melanoma patients stratified as in (C). Curves were analyzed using the Gehan-Breslow-Wilcoxon test.

See also Figure S4.

population remained alive at the end of data collection in this dataset (Figure 6D).

DISCUSSION

While treating tumor immunology as a series of blocked T cell checkpoints has been undoubtedly useful for the generation of therapies (Pardoll, 2012), this report describes a native and intact priming mechanism for anti-tumor $CD8^+$ T cells, apparently intact within multiple tumor models in mice as well as present, by inference, in some human tumors. While the tumor microenvironment itself has been an important site for study of the fundamental mechanisms in T cell inhibition (Gajewski et al., 2013), it is equally important to understand the processes that might generate robust numbers of incoming and activated $CD8^+$ TILs. Here, we have defined a prominent mechanism whereby tumor antigens make their way from the tumor into the dLN for the purpose of driving anti-tumor T cell proliferation. The most numerous migratory cell type with the greatest inherent stimulatory capacity is the $CD103^+$ DC population. These cells traffic tumor antigens in a CCR7-dependent manner to the dLN and this trafficking is critical for effective anti-tumor $CD8^+$ T cell priming.

Previous work has shown intratumoral $CD103^+$ DC to have critical roles as stimulatory, albeit rare, partners for T cells within tumors (Broz et al., 2014). The current study extends this result, showing that these same cells, through expression of CCR7 and trafficking to the LN, also represent key allies for therapies that focus on T cell priming. Furthermore, through the use of $Ccr7^{-/-}$:*Xcr1*-DTR mixed BM chimeras we have been able to further separate the roles of $CD103^+$ DC in the tumor microenvironment from their roles in the dLN. Previously we have shown that $CD103^+$ DC are required for efficient repriming of transferred activated CTLs and subsequent tumor control by blocking LN egress with FTY-720. In this study we show that in addition to this critical role in the primary tumor, $CD103^+$ DC have another crucial role to play in the priming of naive $CD8^+$ T cells in the tumor dLN, which ultimately dictates the ability of CTLs to infiltrate the primary tumor.

Earlier reports using $Batf3^{-/-}$ mice, which result in the loss of both $CD103^+$ and $CD8\alpha^+$ DC (Edelson et al., 2010), demonstrated that this broad lineage was necessary for tumor rejection (Hildner et al., 2008). Further work described robust T cell stimulation by $CD8\alpha^+$ DC purified from the spleens of tumor-bearing mice, promoting these as the critical population for the priming of new $CD8^+$ T cells (Fuertes et al., 2011). Our work is consistent with the *Batf3* result insofar as we found $CD103^+$ DC to be essential, and these rely upon BATF3 (Edelson et al., 2010). Although the $CD8\alpha^+$ may be relevant, our results from directly comparing $CD8\alpha^+$ and $CD103^+$ DC highlight the relatively greater importance of the latter for the triple role of transporting antigen, directly presenting antigen in a highly stimulatory context in vitro and in vivo, and potentially serving as a conduit for handing off antigen to other LN resident DC, including $CD8\alpha^+$ DC. Our study also adds significant nuance to the understanding of LN priming by showing significant, albeit less, trafficking of antigens via $CD11b^+$ migratory DC as well as through the aforementioned hand-off mechanism that may also derive from these cells.

This hand-off pattern of tumor antigen trafficking bears similarities to the import of antigens in skin infections into LN, which take place on one APC subset and are then disseminated to others (Allan et al., 2006). A key difference is that in skin infections, $CD8\alpha^+$ DC were ultimately superior for stimulation of $CD8^+$ T cells when compared head-to-head with $CD8\alpha^-$ DC, which would include the $CD103^+$ DC population. This raises the specter that a solid T cell response in tumors may ultimately profit from activation of the $CD8\alpha^+$ DC alongside the already stimulatory $CD103^+$ DC. Indeed, the previous studies that promoted $CD8\alpha^+$ DC as the critical cells for priming T cells in spleen noted that such priming required signaling through type I interferon (Diamond et al., 2011; Fuertes et al., 2011). To this extent it is intriguing that our real-time imaging showed both DC subsets were frequently together in the same clusters with activating T cells; it is tempting to propose that a concerted dynamic

whereby both DC are activated, perhaps via type I IFN, may produce yet better effectors. Similarly, the other APC populations, while not as robust stimulators of $CD8^+$ T cell activation and proliferation in our assays, may have other, as yet undefined but important, roles in the "quality" of the $CD8^+$ T cell response, as well as other T cell subset activation in vivo, including $CD4^+$ T effectors and T regulatory cells. Future studies should now be in a position to address these issues.

It is also important to consider how different phases of tumor growth may be sampled differently. For example, although it is sometimes postulated that antigen presentation may occur through normal and ongoing tumor cell death, we found that significant import of a 26-kDa pH-stable fluorophore was also blocked by PTX administration and largely abrogated in the absence of CCR7-dependent trafficking. Since this molecule is small enough that it would be expected to be able to drain via lymph to the dLN directly (Sixt et al., 2005), its accumulation in these other myeloid populations in a CCR7-dependent manner very much points to ongoing intratumoral uptake by migratory DC and subsequent trafficking to dLN as cellular "cargo" for direct antigen hand-off. However, this also suggests that there is not typically drainage of small, intact molecules derived from dead tumor cells in the lymph to the dLN, at least in our various mouse models. It remains possible, however, that highly necrotic tumors, particularly as may be the case after certain chemo- and radiotherapy regimes, may more resemble the bolus injection of dead tumor cell debris, which previously implicated $CD169^+$ macrophages in T cell priming (Asano et al., 2011). Furthermore, other mechanisms such as antigen release in the lymphatics may also contribute to a CCR7-dependent acquisition of antigens by LN resident APCs, although that might be expected to result in all LN populations having more uniform and low-level presentation whereas we observe a fraction of cells with high levels, consistent with some form of packet exchange. Future experiments should seek to directly image the cell biology of such a transfer.

This work provides significant rationale for further exploring the CCR7 axis in human cancers as a means to "pull" additional DC populations into LN. In the absence of CCR7 despite the $CD103^+$ DC being present in the tumor at similar levels and being loaded with tumor antigen, anti-tumor T cells were no longer efficiently primed in the dLN, correlating with reduced overall tumor control. Furthermore, intratumoral *CCR7* expression levels were found to be a strong predictor of T cell infiltration and overall survival in human metastatic melanoma, together establishing the critical role of migratory $CD103^+/CD141^+$ DC in LN trafficking and anti-tumor immunity. It will be interesting, as more immunoprofiling of human dLN becomes possible, to correlate TIL infiltration with the presence of CCL21 in sentinel nodes. Yet, given the variety of human melanoma phenotypes, it is important to recognize that LN expression of CCR7 ligands may in some cases provide a route for tumor cells expressing *CCR7* to undertake lymph-based metastasis. Indeed, one recent study demonstrated spontaneous *CCR7* expression in a melanoma cell line (Emmett et al., 2011) and, contrary to our results, another has associated expression of *CCR7* in tumors with more metastasis and worse prognosis in some uveal melanomas (van den Bosch et al., 2013). Thus, although this mechanism appears relevant across multiple mouse and human datasets in our hands, it will be important to consider the exact cells expressing *CCR7* across indications. Similarly, it has been suggested that tumor-specific T cells can be primed directly in tumor tissue in the absence of LN (Thompson et al., 2010). In this regard, though, given the role that $CD103^+$ DC play in both LN priming (this work) and within the tumor (Broz et al., 2014), coupling the viability of these cells to therapy remains a high priority, regardless of the priming site.

How, then, to boost this pathway for therapeutic benefit? Regarding CCR7, it was recently shown that immune complexes stimulate CCR7-dependent DC migration to the LN, which may represent an axis of therapeutic manipulation to drive DC into the LN to enhance anti-tumor T cell priming (Clatworthy et al., 2014). Comparatively, chemo -and radiotherapies, which release tumor antigens, could also increase antigen availability for trafficking $CD103^+$ DC, thus further improving naive anti-tumor T cell responses (Vanneman and Dranoff, 2012). Similarly, coupling of these proposed DC stimulatory therapies with existing immunotherapies, such as checkpoint blockade, will provide exciting opportunities looking forward, especially as it has been noted that several checkpoint blockade therapies, including anti-CTLA4, have heightened effects in the context of DC augmentation strategies (Curran and Allison, 2009). Finally, in noting that $CD11b^+$ DC are relatively weak in trafficking antigens to tumor dLN, we can speculate that there is a "defect" in this axis compared with conventional LN priming; such a defect may ultimately skew T cell responses, particularly as presentation by non-CD103 DC appears important for early $CD8^+$ and $CD4^+$ T cell priming in other contexts (Eickhoff et al., 2015; Pooley et al., 2001). In sum, this work highlights specific DC subpopulations as prominent components for LN priming and provides a roadmap for considering how they contribute to ongoing and effective anti-tumor T cell priming.

EXPERIMENTAL PROCEDURES

Human Specimens

Melanoma samples were obtained from patients at the University of California San Francisco (UCSF) undergoing surgical resection. Experimental protocol CC #138510 was followed and was approved by the institutional review board at UCSF. Informed consent was obtained from patients.

Mouse Strains

All mice were maintained under specific pathogen-free conditions and treated in accordance with the regulatory standards of the NIH and American Association of Laboratory Animal Care standards, and are consistent with the UCSF Institution of Animal Care and Use Committee (IACUC approval: AN106779-01A). OTI transgenic mice (Hoquist et al., 1994) were interbred with CD45.1, *Nur77*^{EGFP} mice (Moran et al., 2011), and *Cd2-RFP* mice (Veiga-Fernandes et al., 2007). *Xcr1*-Venus, *Xcr1*-DTR (Yamazaki et al., 2013), and *PyMT-ChOVA* C57BL/6 mice (Engelhardt et al., 2012) and *Ccr7*$^{-/-}$ C57BL/6 mice (Forster et al., 1999) were bred at UCSF. *Ubc-CreERT2* mice (Ruzankina et al., 2007) were crossed to the *mTmG* reporter strain (Muzumdar et al., 2007) to generate *Ubc-CreERT2 mTmG* mice. C57BL/6 (Simonsen) were used for all ectopic tumor studies.

LN Digestion and DC Isolation

LN were carefully dissected from tumor-bearing or WT mice, and cleaned of fat. For both the PyMTChOVA and B78ChOVA tumors, inguinal and axillary LN were taken as tumor draining. Nodes were pierced and torn with sharp forceps in 24-well plates and incubated for 15 min at 37°C in 1 ml of digestion buffer (100 U/ml collagenase A, 500 U/ml collagenase D, and 20 μg/ml DNAse I in RPMI-1640). After the first 15 min of incubation, cells was pipetted up and down repeatedly, then returned for a second 15-min incubation at 37°C. After

digestion, LN were washed with RPMI-1640 plus 10% fetal calf serum (FCS) and filtered through 70-μm Nytex filters before staining for flow cytometry. When sorting from LN, cells were stained with biotin-conjugated anti-B220 and anti-CD90.2 antibodies, and negative selection was performed with an EasySep Biotin Selection Kit following the manufacturer's instructions before staining.

Flow Cytometry and Antibody Clones

All antibodies were purchased from BD Pharmingen, eBioscience, Invitrogen, BioLegend, and the UCSF hybridoma core, or were produced in the Krummel laboratory. For surface staining, cells were incubated with anti-Fc receptor antibody (clone 2.4G2) and then stained with antibodies in PBS + 2% FCS for 30 min on ice. Viability was assessed by staining with fixable Live/Dead Zombie (BioLegend) or DAPI. Flow cytometry was performed on a BD Fortessa instrument. Analysis of flow cytometry data was done using FlowJo (Treestar) software. Cell sorting was performed using a BD FACS Aria II.

eFluor 670 or VPD450 Labeling of T Cells

OTI T cells were incubated in RPMI-1640 without FCS with 2 μM eFluor 670 (eBioscience) or 5 μM VPD450 (BD Biosciences) for 15 min at 37°C. Cells were then quenched with 2 ml of FCS and washed three times in RPMI-1640 with 10% FCS before use.

T Cell Proliferation Assays

LN cells from *OTI* TCR transgenic mice were isolated and enriched for naive $CD8^+$ T cells by a StemSep CD8 enrichment kit (STEMCELL Technologies). 2×10^4 enriched naive $CD8^+$ T cells labeled with 2 μM eFluor 670 were mixed with either 4×10^3 BM-derived DCs pulsed with or without 25 ng/ml SL8 peptide (OTI) or 4×10^3 unpulsed tumor-derived APCs (unless otherwise noted) in 96-well V-bottom plates for either 12, 48, or 72 hr at 37°C with 5% CO_2, at which point activation was measured by CD69 and Nur77 upregulation and eFluor 670 dilution via flow cytometry.

Human Gene-Expression Analysis

We used previously published microarray and clinical outcome data deposited in the Gene Expression Omnibus (GEO: GSE19234) (Bogunovic et al., 2009) and publicly available TCGA RNA-sequencing and clinical outcome data available at http://cancergenome.nih.gov/ to perform survival and correlation analyses. Statistical analysis was carried out using GraphPad Prism. Survival curves were assessed for statistically significant differences using the Gehan-Breslow-Wilcoxon test, and correlations by calculating the Pearson R value.

SUPPLEMENTAL INFORMATION

Supplemental Information includes Supplemental Experimental Procedures, four figures, and one movie and can be found with this article online at http://dx.doi.org/10.1016/j.ccell.2016.06.003.

AUTHOR CONTRIBUTIONS

M.L.B. and E.W.R. designed and performed the experiments unless specified. A.E.N. and M.B. assisted in analysis of tumor-infiltrating myeloid populations. M.B.H. oversaw imaging experiments. D.M.W. analyzed human expression data. D.B. and N.B. provided helpful advice and datasets. T.K provided reagents. M.F.K. conceived and participated in the design and interpretation of experiments. M.L.B., E.W.R., and M.F.K. wrote, revised, and edited the manuscript.

ACKNOWLEDGMENTS

We thank L. Lanier, J. Roose, and L. Fong for advice and generous sharing of materials. This work was supported by NIH grant U54 CA163123 and R21CA191428. M.L.B. was supported by the Genentech Predoctoral Research Fellowship, the Margaret A. Cunningham Immune Mechanisms in Cancer Research Fellowship Award, and the Achievement Reward for College Scientists Scholarship. E.W.R. was supported by the CRI Irvington Postdoctoral Fellowship. We thank Kaitlin Corbin and Henry Pinkard for imaging assistance and Christine Lin for administrative assistance.

Received: August 21, 2015
Revised: February 8, 2016
Accepted: June 4, 2016
Published: July 14, 2016

REFERENCES

Allan, R.S., Waithman, J., Bedoui, S., Jones, C.M., Villadangos, J.A., Zhan, Y., Lew, A.M., Shortman, K., Heath, W.R., and Carbone, F.R. (2006). Migratory dendritic cells transfer antigen to a lymph node-resident dendritic cell population for efficient CTL priming. Immunity *25*, 153–162.

Asano, K., Nabeyama, A., Miyake, Y., Qiu, C.H., Kurita, A., Tomura, M., Kanagawa, O., Fujii, S., and Tanaka, M. (2011). CD169-positive macrophages dominate antitumor immunity by crosspresenting dead cell-associated antigens. Immunity *34*, 85–95.

Bogunovic, D., O'Neill, D.W., Belitskaya-Levy, I., Vacic, V., Yu, Y.L., Adams, S., Darvishian, F., Berman, R., Shapiro, R., Pavlick, A.C., et al. (2009). Immune profile and mitotic index of metastatic melanoma lesions enhance clinical staging in predicting patient survival. Proc. Natl. Acad. Sci. USA *106*, 20429–20434.

Broz, M.L., Binnewies, M., Boldajipour, B., Nelson, A.E., Pollack, J.L., Erle, D.J., Barczak, A., Rosenblum, M.D., Daud, A., Barber, D.L., et al. (2014). Dissecting the tumor myeloid compartment reveals rare activating antigen-presenting cells critical for T cell immunity. Cancer Cell *26*, 638–652.

Clatworthy, M.R., Aronin, C.E., Mathews, R.J., Morgan, N.Y., Smith, K.G., and Germain, R.N. (2014). Immune complexes stimulate CCR7-dependent dendritic cell migration to lymph nodes. Nat. Med. *20*, 1458–1463.

Curran, M.A., and Allison, J.P. (2009). Tumor vaccines expressing flt3 ligand synergize with ctla-4 blockade to reject preimplanted tumors. Cancer Res. *69*, 7747–7755.

Diamond, M.S., Kinder, M., Matsushita, H., Mashayekhi, M., Dunn, G.P., Archambault, J.M., Lee, H., Arthur, C.D., White, J.M., Kalinke, U., et al. (2011). Type I interferon is selectively required by dendritic cells for immune rejection of tumors. J. Exp. Med. *208*, 1989–2003.

Dunn, G.P., Old, L.J., and Schreiber, R.D. (2004). The immunobiology of cancer immunosurveillance and immunoediting. Immunity *21*, 137–148.

Edelson, B.T., Kc, W., Juang, R., Kohyama, M., Benoit, L.A., Klekotka, P.A., Moon, C., Albring, J.C., Ise, W., Michael, D.G., et al. (2010). Peripheral CD103+ dendritic cells form a unified subset developmentally related to CD8alpha+ conventional dendritic cells. J. Exp. Med. *207*, 823–836.

Eickhoff, S., Brewitz, A., Gerner, M.Y., Klauschen, F., Komander, K., Hemmi, H., Garbi, N., Kaisho, T., Germain, R.N., and Kastenmuller, W. (2015). Robust anti-viral immunity requires multiple distinct T cell-dendritic cell interactions. Cell *162*, 1322–1337.

Emmett, M.S., Lanati, S., Dunn, D.B., Stone, O.A., and Bates, D.O. (2011). CCR7 mediates directed growth of melanomas towards lymphatics. Microcirculation *18*, 172–182.

Engelhardt, J.J., Boldajipour, B., Beemiller, P., Pandurangi, P., Sorensen, C., Werb, Z., Egeblad, M., and Krummel, M.F. (2012). Marginating dendritic cells of the tumor microenvironment cross-present tumor antigens and stably engage tumor-specific T cells. Cancer Cell *21*, 402–417.

Fidler, I.J. (1975). Biological behavior of malignant melanoma cells correlated to their survival in vivo. Cancer Res. *35*, 218–224.

Forster, R., Schubel, A., Breitfeld, D., Kremmer, E., Renner-Muller, I., Wolf, E., and Lipp, M. (1999). CCR7 coordinates the primary immune response by establishing functional microenvironments in secondary lymphoid organs. Cell *99*, 23–33.

Fuertes, M.B., Kacha, A.K., Kline, J., Woo, S.R., Kranz, D.M., Murphy, K.M., and Gajewski, T.F. (2011). Host type I IFN signals are required for antitumor CD8+ T cell responses through CD8{alpha}+ dendritic cells. J. Exp. Med. *208*, 2005–2016.

Gajewski, T.F., Schreiber, H., and Fu, Y.X. (2013). Innate and adaptive immune cells in the tumor microenvironment. Nat. Immunol. *14*, 1014–1022.

Galon, J., Costes, A., Sanchez-Cabo, F., Kirilovsky, A., Mlecnik, B., Lagorce-Pages, C., Tosolini, M., Camus, M., Berger, A., Wind, P., et al. (2006). Type, density, and location of immune cells within human colorectal tumors predict clinical outcome. Science *313*, 1960–1964.

Haniffa, M., Shin, A., Bigley, V., McGovern, N., Teo, P., See, P., Wasan, P.S., Wang, X.N., Malinarich, F., Malleret, B., et al. (2012). Human tissues contain CD141hi cross-presenting dendritic cells with functional homology to mouse CD103+ nonlymphoid dendritic cells. Immunity *37*, 60–73.

Hildner, K., Edelson, B.T., Purtha, W.E., Diamond, M., Matsushita, H., Kohyama, M., Calderon, B., Schraml, B.U., Unanue, E.R., Diamond, M.S., et al. (2008). Batf3 deficiency reveals a critical role for CD8alpha+ dendritic cells in cytotoxic T cell immunity. Science *322*, 1097–1100.

Hoquist, K.A., Jameson, S.C., Heath, W.R., Howard, J.L., Bevan, M.J., and Carbone, F.R. (1994). T cell receptor antagonist peptides induce positive selection. Cell *76*, 17–27.

Huang, A.Y., Golumbek, P., Ahmadzadeh, M., Jaffee, E., Pardoll, D., and Levitsky, H. (1994). Role of bone marrow-derived cells in presenting MHC class I-restricted tumor antigens. Science *264*, 961–965.

Indra, A.K., Warot, X., Brocard, J., Bornert, J.M., Xiao, J.H., Chambon, P., and Metzger, D. (1999). Temporally-controlled site-specific mutagenesis in the basal layer of the epidermis: comparison of the recombinase activity of the tamoxifen-inducible Cre-ER(T) and Cre-ER(T2) recombinases. Nucleic Acids Res. *27*, 4324–4327.

Katayama, H., Yamamoto, A., Mizushima, N., Yoshimori, T., and Miyawaki, A. (2008). GFP-like proteins stably accumulate in lysosomes. Cell Struct. Funct. *33*, 1–12.

Kawakami, Y., Eliyahu, S., Delgado, C.H., Robbins, P.F., Sakaguchi, K., Appella, E., Yannelli, J.R., Adema, G.J., Miki, T., and Rosenberg, S.A. (1994a). Identification of a human melanoma antigen recognized by tumor-infiltrating lymphocytes associated with in vivo tumor rejection. Proc. Natl. Acad. Sci. USA *91*, 6458–6462.

Kawakami, Y., Eliyahu, S., Sakaguchi, K., Robbins, P.F., Rivoltini, L., Yannelli, J.R., Appella, E., and Rosenberg, S.A. (1994b). Identification of the immunodominant peptides of the MART-1 human melanoma antigen recognized by the majority of HLA-A2-restricted tumor infiltrating lymphocytes. J. Exp. Med. *180*, 347–352.

Moran, A.E., Holzapfel, K.L., Xing, Y., Cunningham, N.R., Maltzman, J.S., Punt, J., and Hogquist, K.A. (2011). T cell receptor signal strength in Treg and iNKT cell development demonstrated by a novel fluorescent reporter mouse. J. Exp. Med. *208*, 1279–1289.

Muzumdar, M.D., Tasic, B., Miyamichi, K., Li, L., and Luo, L. (2007). A global double-fluorescent Cre reporter mouse. Genesis *45*, 593–605.

Nakamura, Y., Ishii, J., and Kondo, A. (2013). Bright fluorescence monitoring system utilizing Zoanthus sp. green fluorescent protein (ZsGreen) for human G-protein-coupled receptor signaling in microbial yeast cells. PLoS One *8*, e82237.

Ohl, L., Mohaupt, M., Czeloth, N., Hintzen, G., Kiafard, Z., Zwirner, J., Blankenstein, T., Henning, G., and Forster, R. (2004). CCR7 governs skin dendritic cell migration under inflammatory and steady-state conditions. Immunity *21*, 279–288.

Pardoll, D.M. (2012). The blockade of immune checkpoints in cancer immunotherapy. Nat. Rev. Cancer *12*, 252–264.

Pooley, J.L., Heath, W.R., and Shortman, K. (2001). Cutting edge: intravenous soluble antigen is presented to CD4 T cells by CD8- dendritic cells, but cross-presented to CD8 T cells by CD8+ dendritic cells. J. Immunol. *166*, 5327–5330.

Robbins, P.F., Lu, Y.C., El-Gamil, M., Li, Y.F., Gross, C., Gartner, J., Lin, J.C., Teer, J.K., Cliften, P., Tycksen, E., et al. (2013). Mining exomic sequencing data to identify mutated antigens recognized by adoptively transferred tumor-reactive T cells. Nat. Med. *19*, 747–752.

Ruzankina, Y., Pinzon-Guzman, C., Asare, A., Ong, T., Pontano, L., Cotsarelis, G., Zediak, V.P., Velez, M., Bhandoola, A., and Brown, E.J. (2007). Deletion of the developmentally essential gene ATR in adult mice leads to age-related phenotypes and stem cell loss. Cell Stem Cell *1*, 113–126.

Sixt, M., Kanazawa, N., Selg, M., Samson, T., Roos, G., Reinhardt, D.P., Pabst, R., Lutz, M.B., and Sorokin, L. (2005). The conduit system transports soluble antigens from the afferent lymph to resident dendritic cells in the T cell area of the lymph node. Immunity *22*, 19–29.

Thompson, E.D., Enriquez, H.L., Fu, Y.X., and Engelhard, V.H. (2010). Tumor masses support naive T cell infiltration, activation, and differentiation into effectors. J. Exp. Med. *207*, 1791–1804.

van den Bosch, T., Koopmans, A.E., Vaarwater, J., van den Berg, M., de Klein, A., and Verdijk, R.M. (2013). Chemokine receptor CCR7 expression predicts poor outcome in uveal melanoma and relates to liver metastasis whereas expression of CXCR4 is not of clinical relevance. Invest. Ophthalmol. Vis. Sci. *54*, 7354–7361.

Vanneman, M., and Dranoff, G. (2012). Combining immunotherapy and targeted therapies in cancer treatment. Nat. Rev. Cancer *12*, 237–251.

Veiga-Fernandes, H., Coles, M.C., Foster, K.E., Patel, A., Williams, A., Natarajan, D., Barlow, A., Pachnis, V., and Kioussis, D. (2007). Tyrosine kinase receptor RET is a key regulator of Peyer's patch organogenesis. Nature *446*, 547–551.

Yamazaki, C., Sugiyama, M., Ohta, T., Hemmi, H., Hamada, E., Sasaki, I., Fukuda, Y., Yano, T., Nobuoka, M., Hirashima, T., et al. (2013). Critical roles of a dendritic cell subset expressing a chemokine receptor, XCR1. J. Immunol. *190*, 6071–6082.